Energy & Buildings 262 (2022) 112012

Contents lists available at ScienceDirect

Energy & Buildings

journal homepage: www.elsevier.com/locate/enb

A new tool and workflow for the simulation of the non-image forming effects of light

Marshal Maskarenj [a], Bertrand Deroisy [b], Sergio Altomonte [a,*]

[a] Architecture et Climat, Louvain Research Institute for Landscape, Architecture, Built Environment, Université catholique de Louvain, Louvain-la-Neuve, Belgium
[b] Belgian Building Research Institute, Brussels, Belgium

ARTICLE INFO

Article history:
Received 30 November 2021
Revised 5 February 2022
Accepted 5 March 2022
Available online 8 March 2022

Keywords:
Daylight
Non-image-forming effects
Spectral sky simulation
Grasshopper
Integrative lighting
Integrated lighting solutions

ABSTRACT

Other than supporting vision, light plays an important role in regulating human circadian rhythms through its non-image-forming (NIF) effects. Simulating potential NIF stimulation from daylight indoors, however, is a challenging task, requiring the continuous evaluation of luminous exposures at the eye, which are affected by changing sky's spectral power distributions at a location, time of day and year, and estimation of the sky patches' contributions at a viewing position, which dynamically vary through a space. Existing multi-channel NIF simulations tools use measured or pre-computed spectral sky data. Yet, these are difficult to obtain with flexible spatio-temporal resolution. To address this challenge, and dynamically estimate a range of NIF metrics, we developed a tool and workflow based on 17 original Python-scripted Grasshopper components. This paper illustrates the design and development of the tool and workflow, also presenting an example of practical application to evaluate the yearly variations of potential NIF stimulation from an interior position or under an unobstructed sky. This is the first step to propose more robust building design and modelling concepts, beyond conventional visual comfort issues, and to adequately balance lighting energy use with occupants' comprehensive needs, while connecting daylighting and electric lighting systems and controls within integrated solutions.

© 2022 Elsevier B.V. All rights reserved.

1. Introduction

Other than supporting the visual needs of humans, light plays a fundamental role towards their health and well-being through its *non-image forming* (NIF) effects (also deemed *non-visual*, since they originate in the eye but are separate from vision), which regulate many neuro-physiological, neuro-endocrine, and neuro-behavioural processes required to maintain *homeostasis* [1,2]. Among non-image forming effects, adequate exposure to luminous stimulation contributes, in the *short term*, to suppress the pineal hormone melatonin (whose secretion is associated with the body preparing for sleep), stimulate the production of cortisol, regulate heart rate, core body temperature, and many neuro-physiological processes related to alertness, arousal, cognitive performance, etc. In the *long term*, NIF effects can drive several neuro-behavioural functions, for example enabling the synchronization of the endogenous *circadian clock* to the daily cycle of light and dark [2]. Circadian rhythms are evolutionarily-developed biological phases that are regulated by the *suprachiasmatic nuclei* (SCN) in the hypothalamus. In humans, the SCN exhibit an endogenous periodicity oscillating between 23.7 and 25.1 hours [3], hence requiring regular resetting through external cues to prevent its free-running from the natural 24-hour light–dark cycle [4], and avoid many aspects of physiology and behaviour (e.g., social life, sleep-wake patterns, etc.) to become de-synchronized from each other [5]. Asynchrony between bodily and natural rhythms may lead to circadian misalignment resulting in, among others, decreased performance, sleep disorders, and a higher risk of several diseases [6,7].

Non-image forming effects are mainly attributed to a class of *intrinsically photosensitive Retinal Ganglion Cells* (ipRGCs) that achieve photoreception through expression of *melanopsin*, an opsin photopigment [8,9], based on the intensity, duration, spectrum, timing, and history of luminous exposure [10,11]. NIF responses have been found to also be influenced by extrinsic signals from the rods and the three classes of cones (S-, M-, L-cones) present in the human retina. Each route of light detection has its own spectral sensitivity, defined by the efficiency of the respective photopigment. Inputs from the five photoreceptors are combined by the retinal wiring, and within ipRGCs, to create a context-dependent integrated signal that is sent to neural centres [12]. This brings a new dimension to lighting design, one that focuses on the potential to improve the well-being of individuals. However, predicting the NIF effects of

* Corresponding author.
E-mail address: sergio.altomonte@uclouvain.be (S. Altomonte).

https://doi.org/10.1016/j.enbuild.2022.112012
0378-7788/© 2022 Elsevier B.V. All rights reserved.

light presents many challenges, since this requires a complete modelling of a complex interplay between several factors that can vary under a range of conditions. These factors are related to the *luminous stimulus* itself – e.g., its photometric, spatial, and temporal characteristics – to the *individual*, such as prior light history and state of health (e.g., sleep deprivation) [13], but also to the *physical features* of indoor and outdoor spaces.

Although there are widely accepted metrics and tools for quantifying aspects of *lighting sufficiency* and, to some extent, for evaluating the risks of *visual discomfort* (e.g., glare) inside buildings, and their potential implication on energy performance, the identification of an inclusive modelling workflow for predicting and assessing the NIF qualities of a luminous environment still proves elusive.

Among several existing *metrics* that have recently been proposed for evaluating the NIF effects of light, this study focuses on the CIE-adopted α-opic *melanopic equivalent daylight illuminance* [14] (abbreviated as melanopic-EDI, or *mEDI*, and denoted as $E_{v,mel}^{D65}$), the *M/P (Melanopic / Photopic) ratio*, along with the *Circadian Light (CLa)*, and the *Circadian Stimulus* (CS) [6,15,16]. For the *calculation* of these metrics, which are presented more in detail in the following Section 2.1., spreadsheet-based tools are available [17,18], which use as inputs the illuminance values and spectral characteristics of the (natural and electric) light sources interacting in a scene.

In terms of building performance *simulation*, two platforms are increasingly used by lighting designers to model lighting measures (i.e., the traditional illuminance, or *photopic* lux) alongside the NIF effects of light [19,20]: *ALFA* [21] and *LARK* [22]. ALFA – a plug-in to Rhinoceros 3D – utilises an 81-channel simulation based on pre-computed spectral sky irradiance (using *libRadtran*) and luminaire data. LARK – a Grasshopper-based workflow featuring originally-scripted components [23] – uses measured spectral irradiance sky data, in a 9-channel simulation, to calculate photopic lux (based on the CIE photopic curve V(λ)) and circadian outputs [12,24].

Although appropriate factors may be used to convert between the metrics estimated by these spectral simulation platforms, both these tools have been developed before the adoption of the CIE melanopic-EDI (mEDI). In addition, a relevant challenge remains in accurately predicting the NIF effects of light in the absence of spectral daylight measurements from an unobstructed sky. Also, since the occurrence of NIF effects inside a space often derives from a combination of daylight and electric light, another fundamental question is represented by the evaluation of the potential NIF stimulation resulting from the portion of sky vault that is effectively visible from a certain view angle and position. This illustrates the critical limitations of existing modelling capacities, particularly in the case of complex luminous environments characterized by the integration of daylight (e.g., due to dynamically changing sky conditions) and electric lighting (e.g., to increase energy efficiency), as it is often the case in our buildings. There is, therefore, scope to develop more robust algorithms to estimate daylight spectral power distributions (SPD) more accurately, at various points in time, for different locations and viewing positions, to quantify the potential occurrence and magnitude of NIF effects inside spaces. A complete workflow that streamlines the simulation process for designers could also be beneficial to facilitate decisions across the various stages of design and occupancy of a building.

To respond to these challenges, this paper presents a new open-source workflow and simulation tool, *OWL – Occupant Well-being through Lighting*, along with originally scripted Rhino Grasshopper (GH) components. The OWL tool has been developed to estimate the SPD of the sky from an observer's point of view inside a space at any location and point-in-time, taking available weather data as input. The workflow can be used in the absence of measured instantaneous sky SPD data, whereas discretized spectral power distributions from relevant sky positions are combined towards the evaluation of a series of NIF metrics.

The paper is structured as follows. Following this introduction, Section 2 presents the metrics and methods of this study, providing a synthesis of the literature on measuring NIF effects and describing the process for the development of OWL and the implementation of its computational workflow. The tool is presented in Section 3, illustrating in detail the various components scripted in Rhino Grasshopper. An example of practical application of OWL is then given in Section 4 for a generic shoe-box model simulated at the coordinates of London. Finally, the potential impacts of the OWL tool and workflow in research and practice are discussed in Section 5, to facilitate the design and operation of more comfortable, healthy, and energy efficient buildings.

2. Metrics and methods

2.1. NIF metrics in building design and simulation

The rod and cone photoreceptors provide vision through expression of light-sensitive retinal proteins, or opsins: *rhodopsin* (rods), *cyanopsin* (S-cone), *chloropsin* (M-cone), and *erythropsin* (L-cone). The ipRGCs comprise a third class of photoreceptors that communicate directly to the brain, which similarly convert the luminous stimuli received at the eye to a neurochemical signal through *melanopsin* [25].

Each photoreceptor is characterized by its own spectral sensitivity. The rod, S-cone, M-cone, and L-cone sensitivities peak at about 507 nm, 448 nm, 545 nm, and 569 nm, respectively, also considering pre-receptoral filtering in the retina. For melanopsin, the peak sensitivity has been reported to be around 480–490 nm, towards the blue part of the spectrum [12,24]. The ipRGCs combine their melanopsin-induced *intrinsic* response with *extrinsic* retinal inputs that originate from cones and rods [26]. For this reason, the term 'melanopic-response' refers to the *intrinsic* response from ipRGCs, whereas 'ipRGC-response' refers to the combined *intrinsic* and *extrinsic* response [27]. In circadian regulation, the melanopic response is purely non-visual, but the ipRGC-response is a combination of visual and non-visual processes [28,29]. The balance between the intrinsic and extrinsic inputs towards the combined ipRGC-response, however, still lacks complete understanding, and the NIF metrics that are described below only partially address the different characteristics of the 'melanopic-response' and 'ipRGC-response' ranges [27].

A *metric* refers to a system of related measures that facilitate the quantification of a phenomenon. Several measures and criteria are featured in building standards and rating systems towards supporting building design development and performance evaluation. However, since the combined melanopic and ipRGC response has not yet been fully characterized [27], it is only recently that international regulations have started to include metrics for predicting and quantifying the occurrence of non-image forming effects of light. Among these, the CIE-adopted *melanopic equivalent daylight illuminance* (mEDI), denoted as $E_{v,mel}^{D65}$, is a melanopsin-focused subset of the α-opic EDI set of metrics (where α stands for the opsin expressed by each photoreceptor [14]). The α-opic action spectrum is used to weigh the absolute SPD of a light source to the CIE standard illuminant D65, representing average daylight [27]. The set of α-opic metrics adopted by the CIE (specifically, the mEDI) is consistent with the method employed for estimating photopic sensitivity [13]. However, by only including the sensitization of the melanopic photoreceptors, and not the downstream effect on circadian response, this metric is closer to the melanopic response than

the combined *ipRGC influenced light* (also termed iIL) response involving all classes of photoreceptors [27].

Another NIF metric, hinting at the suppression of melatonin as a proxy for circadian response, is the *Circadian Stimulus* (CS), proposed by the Lighting Research Centre (LRC) at Rensselaer Polytechnic Institute [6,15,16]. The CS predicts the melatonin suppression following sustained exposure to a light stimulus, primarily accounting for the intrinsic melanopic response, but also including a certain input from the S-cones. This metric is closer to the ipRGC-response since the effects considered are a combination of visual- and non-visual processes. However, CS only evaluates the potential of melatonin suppression and cannot be robustly used for estimating other NIF effects (e.g., level of alertness throughout the day) [30].

A slightly older metric, which is also featured within the criteria of the International WELL Building Standard [31], is the *Equivalent Melanopic Lux*, or *EML* [12]. This metric does not quantify the 'biological' potency of light, it only estimates melanopic spectral responses, which play a role towards circadian entrainment. The EML uses a similar calculation method as mEDI, and is a melanopic-subset of the EDI approach, which can also evaluate the response of the other four opsins. EML can be translated to mEDI, its value being around 1.104 times $E_{v,mel}^{D65}$ [32]. Alongside the EML, another metric that offers an indication of the potential alerting (or calming) effects of a light source is the *M/P ratio* [33], where 'M' and 'P' stand for *melanopic* and *photopic* lux. Light sources with a spectrum shifted towards longer wavelengths (red-dominated), and a M/P ratio lower than 0.35, are considered calming. Light sources with a spectrum shifted towards shorter wavelengths (blue-dominated), and M/P ratio higher than 0.9, are considered alerting. For proper circadian entrainment, people should be exposed to an alerting spectrum (high EML and M/P ratio) in the morning, and to a calming spectrum (low EML and M/P ratio) at later hours of the day [33].

The *Equivalent Melanopic Lux* and the *M/P ratio* are the NIF metrics implemented in the ALFA simulation tool, while the LARK platform produces melanopic spectral response curve-weighted luminance renderings and illuminance values [20,34] adopting, respectively, the melanopsin spectral sensitivity curve published by Lucas et al. [12] (*Lucas lux*), and the circadian spectral sensitivity curve published by Rea [24] (*Rea lux*). Both tools, ALFA and LARK, rely on spectral reflectivity and transmissivity data of the materials (e.g., surfaces, glazing) present within an internal luminous scene, with ALFA offering a spectral material library that is compatible with the International Glazing Database (IGDB) [35].

2.2. Scripting the tool

OWL (*Occupant Well-being through Lighting*) is based on 17 originally created Python-scripted Grasshopper (GH) components, and it features a user-friendly workflow structured on an intuitive dashboard.

The luminance of various positions of the sky dome is evaluated using the Perez sky model [36]. Yet, the user may choose to alternatively run the simulations based on CIE standard skies [37]. The luminance at various positions from an observer's viewpoint is evaluated through Radiance image-based simulations. Using the approach proposed by Diakite-Kortlever and Knoop [38], the luminance data at different sky patches is converted to corresponding Correlated Colour Temperature (CCT) data, and these are used to calculate respective patch-SPDs using the recommendations of the CIE standard 015 on colorimetry [39]. The various sky patches are then assumed as separate light sources – each with its own SPD providing individual luminous contribution – and merged to generate relative-combined SPD data for the entire sky dome/viewfield using a similar procedure to that adopted by the LRC, whereas a Circadian Light Combined Calculator estimates the relative-combined SPD from different light sources using their spectral characteristics and respective illuminance contributions [17]. Therefore, the relative-combined SPD data, under an unobstructed sky or at the observer's viewpoint, only need weather file data and time of the year/day as inputs, along with Rhino geometric definitions. The SPD data can be used for evaluating α-opic metrics (mEDI, among others) using the approach of the CIE S 026 standard [13], and circadian metrics (CS, among others), using the LRC worksheet [16]. The data can also be employed as additional spectral input for existing simulation platforms for an unobstructed view of the sky vault. To complement the information presented in this paper, all the original Python-scripted Grasshopper components, and the proposed workflow, are freely available to the research and design community under creative commons open access license on https://marshalmaskarenj.github.io/OWL_Web/index.html.

3. OWL: Occupant Well-being through Lighting

3.1. A workflow for sky spectral distributions

To quantify the potential non-image forming effects available within an internal visual scene, alongside the stimulation obtainable under an unobstructed sky, this paper uses the melanopic metrics *(melanopic irradiance, melanopic-ELR, melanopic-DER*, and *melanopic-EDI)* that are subsets of the CIE α-opic units of measure [13], as well as the circadian metrics (*Circadian Light* and *Circadian Stimulus*) developed by the LRC.

A framework for the evaluation of the melanopic *Daylight Efficacy Ratio* (mDER, denoted as $\gamma_{mel,v}^{D65}$), and the ratio of melanopic-weighted radiant flux to photopic-weighted radiant flux (melanopic *Efficacy of Luminous Radiation* or mELR, denoted as $K_{mel,v}$), was proposed by Diakite-Kortlever and Knoop [38]. In their study, the photopic-weighted radiant flux represented the maximum spectral luminous efficacy of radiation for photopic vision. Their framework evaluates NIF metrics through a methodology where sky luminance is converted to sky CCT using existing models, and sky SPD is reconstructed from CCT data in accordance with the CIE 015 standard [39]. Further, the reconstructed SPD is used to calculate NIF metrics according to the CIE S 026 standard [40]. The framework proposed by [38] is presented as workflow (a) in Fig. 1.

In workflow (a), the CIE 015 standard document provides a conversion protocol for reconstructing SPD data from CCT between 4000 and 25000 K, where the CCT values are calculated from luminance data using the existing luminance-to-CCT models presented in the study [38]. Using the CIE 015 protocol, relative SPD can be generated for wavelengths in the range between 300 and 830 nm, normalized with the data at 560 nm. Also referred in workflow (a), the CIE S 026 document provides a procedure for evaluating α-opic NIF metrics when illuminance and spectral data of the source are available.

A previous publication by Diakite-Kortlever and Knoop [41] proposed sky-discretization for increasing data resolution, where sky luminance (measured or simulated) is discretized into equal-sized patches before the luminance-to-CCT conversion. While the first step of workflow (a) features sky luminance, based on [41], this may also be assumed as discretized sky luminance, where the additional steps of the workflow indicate the conversion of each patch luminance to the respective CCT, and further to SPD for evaluating the CIE-recommended NIF metrics. Workflow (a), thus, provides a theoretical framework for evaluating NIF metrics using available weather data. However, since estimated data are

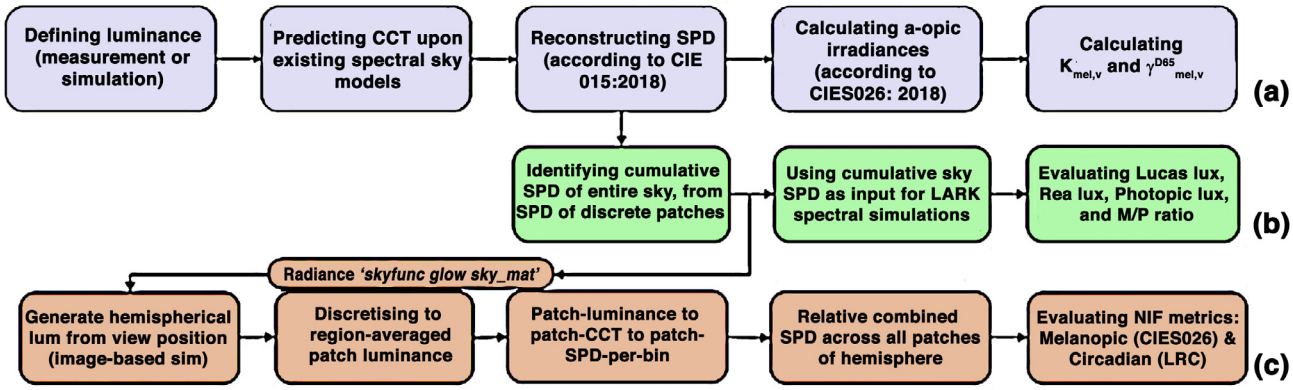


Fig. 1. (a) Workflow proposed by Diakite-Kortlever and Knoop [38]; (b) Proposed extension of LARK workflow by using pre-evaluated sky SPD; (c) Proposed OWL workflow for evaluating SPD at a view point and estimating NIF metrics.

influenced by all the sky patches across the sky hemisphere, the results can only represent the potential NIF effects of daylight under an unobstructed sky, when an observer is looking at the entire sky dome while facing the zenith.

For evaluating NIF metrics at an indoor scene, ALFA and LARK can be used. While ALFA uses *libRadtran* for modelling sky irradiance as spectral input for the evaluation, LARK requires point-in-time spectral sky data, which can be, however, challenging to obtain at proper spatio-temporal resolution. Yet, since EnergyPlus Weather (EPW) files are widely available, there is a potential to connect workflow (a) with LARK, whereas the generated sky SPD can be used as representative spectral input. This is presented as workflow (b) in Fig. 1.

An indoor view does not include all parts of the sky, but only those sky patches within (or nearby) the observer's field of view that contribute to the spectral optical radiation incident at the eye, or influence it through ambient bounces. This offers an opportunity to diverge from workflow (a), and use luminance distribution at an observer's view as the starting point for evaluating NIF metrics. This luminance distribution can be generated through simulation, for then being converted to CCT and further to SPD for the estimation of NIF metrics at the view. This procedure is presented as workflow (c) in Fig. 1. The lack of combined spectrally and spatially resolved optical properties for many surfaces in the literature, however, limits workflow (c) to direct rays, hence only the luminance inputs from the sky fraction that are directly visible to an observer are currently used for the NIF evaluation. Luminance contributions arising from inter-reflections are not estimated, while reflected light from surrounding external surfaces should also be considered for a more comprehensive evaluation. The consideration of only direct rays (without inter-reflections) also means that direct view to a portion of the sky is necessary for estimating NIF metrics under the proposed workflow.

The hemispherical luminance map at an observer's view, serving as the starting point for the view-based NIF evaluation in workflow (c), is generated via Radiance image-based simulation. Here the *'skyfunc glow sky_mat'* parameter in the Radiance sky file includes average SPD per channel (generated from modelled SPD in workflow (a)), which is used to generate a spectral light source in Radiance *gensky*. Ambient bounce is set at 0 to eliminate luminance contributions from obstructed positions, and the direct-sky luminance map is discretized to equal patches with direct-sky contributions only. Luminance of each view-patch is then converted to CCT, and thereafter to SPD for evaluating NIF metrics, similar to workflow (a). Since the starting step of workflow (c) (luminance map) takes as input the output from workflow (a) (average SPD per channel of the sky), workflow (c) may also be considered as a view-based extension of workflow (a).

The version of workflow (c) presented in this paper is limited to NIF evaluation using only direct-sky components of daylight, while NIF contributions from positions representing internally and externally reflected daylight components are not considered. With deeper understanding of spectral interactions of light in a scene, and image-based spectral simulation protocols, a future development of workflow (c) will incorporate NIF contributions from all sky positions, based on direct and inter-reflected rays.

3.2. Grasshopper components

The Rhinoceros software provides the Grasshopper (GH) interface for visual scripting, which supports designers in performing customized design evaluations. The Ladybug suite of GH plugins [23] can be used for environmental analysis, and ClimateStudio [42] also offers a GH interface for advanced simulations. LARK [22] is also a GH workflow for performing spectral daylight simulation. To support the theoretical workflows (a) through (c), we chose GH as the scripting platform, whereas some components from Ladybug tools [23] have also been integrated in the analysis. All the originally scripted components were developed using *GHPython* [43] and *GH_CPython* [44], which are modular Python-based GH components that allow customization of inputs and outputs. The various components, and their modelling criteria, are briefly presented in the following sections. A full description is available as an open access resource on the OWL webpage.

3.2.1. Extracting weather parameters

We scripted two components, *OpenEPW_loc* and *OpenEPW,* to extract static headers and temporally dynamic data from EnergyPlus Weather (EPW) files. An EPW file is a text-based file that contains 8 rows of static data corresponding to location, design conditions, and daylight-saving parameters, followed by 8760 rows of data corresponding to each hour of the year. Each of the hourly dataset rows are comprised of 35 environmental parameters, corresponding to temperature, irradiance, illuminance [45], etc. The *OpenEPW_loc* component takes a weather file as input, and extracts location name, latitude, longitude, time-zone, and elevation data, respectively. While connected to the weather file, the *OpenEPW* component uses hour-of-year (HOY) and output-index as inputs for extracting corresponding data, where output-index is a numeric value between 1 and 35, corresponding to type of environmental parameter.

3.2.2. Solar altitude and azimuth

The *SunPos* component uses the location data from *OpenEPW_loc,* along with hour-of-day and day-of-year, to generate location and time specific solar altitude and azimuth. Validated with available tools [46–48], and with the GH Ladybug *Sunpath* component [23], *SunPos* nodes are tailored to the workflows designed.

3.2.3. Generating sky patch luminance

The *PerezSky* and *CIE_Skygen* components use the Perez all-weather model [36] and the CIE standard sky model [37], respectively, for generating luminance data across various sky positions. 145 discrete positions, corresponding to the model used in Daysim [49] adopted from the Tregenza sky subdivision scheme [50], are used as altitude/azimuth combinations for evaluating respective sky luminance data. The *PerezSky* component generates the 145-luminance output as a function of: solar altitude, solar azimuth, zenith luminance, horizontal diffuse radiation, direct normal radiation, optical air mass, and extra-terrestrial direct normal radiation. The Solar altitude/azimuth data are taken from the outputs of *SunPos,* while the other environmental parameters for a given HOY are taken from *OpenEPW* by setting 'index' at 20, 16, 15, and 12, for zenith luminance, diffuse horizontal radiation, direct normal radiation, and extra-terrestrial direct normal radiation, respectively. The optical air mass parameter is user-defined for parametric simulations at various turbidity values (the default value is set to 2, referring to a solar elevation angle of 30° [51]). The *CIE_Skygen* component also generates 145 luminance values as output, as a function of solar altitude, azimuth, zenith luminance, and sky type. The first three data for a given HOY are taken from the *SunPos* and *OpenEPW* components, respectively, akin to the *PerezSky*, while the CIE sky model is user-defined for simulations at various sky types. This parameter takes a value between 1 and 15, which corresponds to the 15 CIE sky types for a range of overcast, uniform, intermediate, and clear conditions [37].

3.2.4. Generating view-based luminance maps

Discretized luminance data from Radiance image-based simulation serve as the starting point for workflow (c). To generate view-based luminance maps, two components, *SPD2spectral* and *3CspectralSky*, were scripted to generate the spectral sky definitions used in Radiance image-based simulations.

SPD2spectral calculates SPD averaged-per-channel data when SPD data are provided as input. This component has a functionality similar to the 3-channel sky approach of the LARK's *SpectralMaterials* component, where input SPD is binned in the red, green, and blue regions of the spectrum, and the binned averages are normalized with the SPD peak value to generate average SPD per channel. Since our workflow considers only relative SPD data in its evaluation, the peak value is always 1. The 586–780 nm range is considered as the red (R) region, the 498–586 nm range is considered as the green (G) part, and the 380–498 nm range is considered as the blue (B) region of the visible spectrum [22].

The *3CspectralSky* component takes in channel data from *SPD2spectral* and generates a sky file for Radiance simulations. Other inputs are: location (from *OpenEPW_loc*), Radiance sky type, time (Hour/Day/Month), solar position (from *SunPos*), and environmental parameters of direct normal radiation and diffuse horizontal radiation (from *OpenEPW*). The average SPD per channel data shapes the '*skyfunc glow sky_mat*' parameter of the sky file, which is one of the key inputs while generating luminance maps through the Honeybee's *Run Daylight Simulation* and *Image based simulation* components.

The luminance maps generated by the Honeybee *Run Daylight Simulation* component are in high dynamic range image (HDRi) format. An HDR file of m-by-n pixels in RGB comprises pixel data in a 3-dimensional numeric array of m-by-n-by-3, where 3 represents the layers for each of the RGB channels. Each cell of the array in a HDR file can store a high range of data, between 0 and '*Inf*', which is wide enough to accommodate the characteristics of human vision [52]. It is worth noting that an 8 bit RGB file format (such as the.JPEG) can stores pixel data between 0 and 255 for each channel, with a range limited to just two orders of magnitude. Through post-processing, the per-pixel data from HDR files can be clustered into 2-dimensional regions, which can then be averaged to reduce the data resolution [53] and increase computational speed. This way, the luminance detail from a user's view is not compromised, and the CCT of each region can be calculated from discretized luminance data, akin to the protocol used for sky-luminance distribution.

The *HDR2DiscreteLumEx* component reads the HDR luminance maps and extracts actionable data. It discretizes the HDR luminance map to 145 constituents, representing equal-sized regions in an observer's hemispherical view, with the centre representing the foveal point. Along with the luminance map, this component takes as input a multi-layered .mat file of masks for each of the discretized regions, and a single-layer mask file representing the field of view: fisheye/binocular/human-vision (interpreted from [54]).

HDR2DiscreteLumEx was scripted with *GH_CPython* [44] as this component requires additional Python libraries (such as *NumPy*, *SciPy*, *OS*, and *matplotlib*) not supported by *GHPython*. On the given HDR file, this component performs the command *pvalue -o + u -h -H HDR_file > output.txt*, which generates a text file with factored luminance data in a linear array for the 3 RGB channels. Further, the text file is read as linear data and restructured to 2D arrays, and the factors of 0.299, 0.587, and 0.114 are multiplied to the red, green, and blue layers, respectively, to generate a grayscale factored luminance map. A factor of 179 is multiplied to each pixel for generating the actual luminance data. Once the HDR is converted to a map of luminance data, a field-of-view mask representing either a fisheye, binocular, or human-vision, is factored in with the luminance data. Further, the luminance map is multiplied with a multi-layered region mask, with each layer representing a discretized patch of the hemisphere, and average luminance of each region is extracted to yield 145 values. These values correspond to the average luminance from each of the 145 patches. This component generates a map of masked luminance data, a map of region average luminance data, and a matrix of 145 averaged luminance values. The matrix generated here is the view counterpart to the outputs from *PerezSky* or *CIE_Skygen* components, and is used for the next steps of the workflow.

3.2.5. Converting patch luminance to CCT

Diakite-Kortlever and Knoop [38] compared long-term spectral sky data measured in Berlin with four existing luminance-related spectral sky models described in the literature [55–58], and recommended the most suited model under various conditions. These models express the colorimetric distribution of daylight across the sky dome, evaluating the CCT of a sky patch from its luminance. Further, the most appropriate model for the real data was evaluated using the Mean Absolute Error (MAE); that is, the measured and modelled CCTs for various ranges were compared, and the model with the minimum MAE for a given CCT range was recommended. For clear skies with CCT between 4000 and 10000 K, the Chain (2004) model [57] was considered the most suitable; for CCT ranging between 10000 and 12500 K, the Rusnak model [58] was suggested; the Chain (1999) model [56] was, finally, recommended between 12500 and 25000 K. Through numerical analysis of these recommendations, we identified the luminance thresholds in applying the most suitable model across various luminance ranges and evaluating the CCT for a sky patch from the luminance data. The Chain (1999) model was found applicable for sky patch luminance below 3172 cd/m^2, the Rusnak (2014) model for lumi-

nance between 3172 and 5200 cd/m^2, and the Chain (2004) model for luminance higher than 5200 cd/m^2.

To emulate the referred luminance related spectral sky models [56–58], along with the recommended protocol for model selection [38], we scripted a component termed *SpectralSkydome*. For every input datapoint representing a luminance value, this component identifies the suitable model and provides CCT and model index as output. In the workflow, the component is fed 145 datapoints as input, these representing the luminance distribution across 145 sky patches. For a given sky luminance distribution dataset fed to the component, the evaluated CCT for each patch of the dataset is provided. For the view counterpart workflow, we scripted a similar component termed *SpectralViewdome*, which performs similar evaluations but with one add-on: a luminance threshold is allowed to separate the direct sky luminance contributions from the reflected components. This is because the luminance-to-CCT models are applicable only to sky cases, without considering the reflected luminance contribution (internal and external). *SpectralViewdome* returns 0 as CCT for patches with average luminance under the defined threshold.

3.2.6. Converting patch CCT to SPD

The CIE 015 standard [39] provides the protocol for reconstructing daylight's CCT to SPD, with spectral resolution of 5 nm across the 300–830 nm range. The model is applicable for CCT values between 4000 K and 25000 K. For a given CCT, the model evaluates 107 datapoints corresponding to the relative spectral power distribution [S(λ)] of daylight, for every 5 nm bin. The distribution is normalized for the value of 560 nm; as such, the normalized SPD at 560 nm is set to the value of 100 (exactly) for any reconstructed SPD curve. Fig. 2 plots the SPD curves between 380 and 830 nm, for CCT values in the 4000–25000 K range.

We scripted a component, *CCT2SPD*, based on the models featured in the CIE 015 standard. For any given CCT input value between 4000 and 25000 K, this component generates 107 datapoints corresponding to the relative SPD for every 5 nm. For the view counterpart workflow, we scripted *ViewCCT2SPD*, which performs a similar evaluation but for one exception: since *SpectralViewdome* returns 0 as CCT output for patches without direct sky luminance contribution, *ViewCCT2SPD* returns a null-array for such patches.

3.2.7. Generating relative-combined SPD

In our workflow, the component *CCT2SPD* (or *ViewCCT2SPD*) generates 145 sets of SPDs corresponding to the 145 sky patches. However, to be useful in evaluating NIF metrics, or as spectral input for LARK, the individual contributions of SPD and the illuminance from each hemispherical patch need to be cumulated over the entire sky dome (or view hemisphere). For this, the approach adopted by the LRC [17] is used, and the relative-combined SPD for the entire hemisphere in both cases is calculated by considering each equal-sized patch as an individual light source. Along with the relative SPD of each patch, their average luminance is calculated, and the illuminance contribution of each patch is identified by factoring their subtended solid angle. Each of the 145 patches has a solid angle of 0.0433 sr (a cone with a 13.5° apex angle) [59], which is further factored with the sine of their altitude (or foveal) angles. The patch luminance factored with 0.0433 sr, along with the sine of individual altitudes or foveal angles, yields the illuminance contribution for each patch. The component *RelativeCombinedSPD* takes the 5 nm separated SPD data from *CCT2SPD* (15515 values representing all 145 patches), along with luminance contributions from each of the 145 patches (from *PerezSky, CIE_Skygen*, or *HDR2DiscreteLumEx*) as inputs, and provides the relative-combined SPD (176 datapoints through 380–730 nm range with step-size of 2 nm) and net illuminance.

The workflow presented so far enables to use available EPW weather files to generate hourly SPD on a horizontal plane under an unobstructed sky, or on a vertical plane at the observer's eye facing a visual scene. This model-generated SPD data may be used for evaluating NIF α-opic metrics or circadian metrics (workflow (a) or (c)). The sky SPD may also be used for LARK simulations (workflow (b)). At each timepoint, the sky SPD is generated early in the workflow for the entire sky hemisphere rather than only for those sky patches that are visible to the observer from their location in the space. This allows the flexibility to continuously estimate NIF metrics while moving the viewing position and angles without requiring any additional computation. It should be noted that evaluating the relative-combined SPD for the entire sky hemisphere takes less than 1% of the total workflow running time.

3.2.8. Estimating NIF metrics

To estimate α-opic metrics based on the CIE S 026 standard, we scripted a component termed *CIES026_aopic*. This component takes

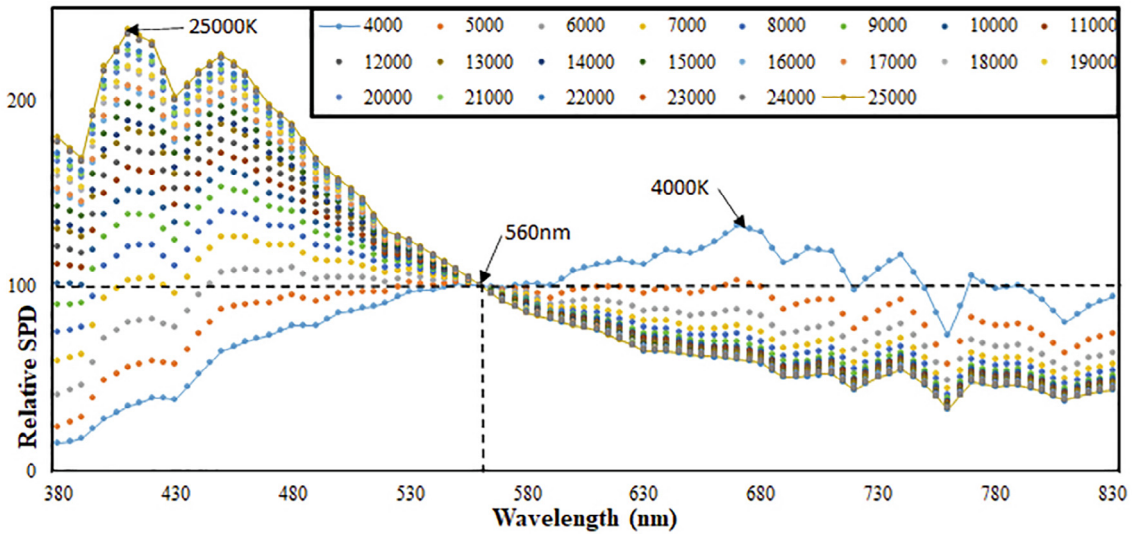


Fig. 2. Reconstructed relative SPD between 380 and 830 nm for different CCTs, according to the models in CIE 015: 2018.

as input the incident SPD and the net illuminance data (both from the outputs of *RelativeCombinedSPD*) along with an indicator of the α-type. By factoring the α-opic and photopic sensitivity curves with relative-combined SPD data, the following are evaluated: net *Illuminance*, α-opic *Irradiance*, α-opic *Efficacy of Luminous Radiation* (ELR), α-opic *Daylight Efficacy Ratio* (DER), and α-opic *Equivalent Daylight Illuminance* (EDI). Although *CIES026_aopic* can provide all the α-opic sets of metrics, only the melanopic evaluations are considered in the example of application presented in the following section, where we have estimated melanopic EDI and Illuminance to evaluate the M/P ratio as the key indicators. We also scripted a component termed *circadLight*, which uses the incident SPD and the net illuminance data (both from the outputs of *RelativeCombinedSPD*) to evaluate the *Circadian Light* (CLa) and the *Circadian Stimulus* (CS). All the components that have been originally scripted for the OWL tool, and the full *Luminance-to-NIF* workflow described above, are illustrated in Fig. 3.

A dashboard has also been created to visualize and control all parameters necessary for performing the simulations (Fig. 4). The independent parameters include: location (through definition of the EPW File), view (which includes a camera and a target in a Rhino scene), analysis period (hour, day, month), field-of-view mask (binocular/human-vision/fisheye), and Radiance sky-type (−s, +s, −c, −i, +i, −u). The dependent parameters include: sky SPD at a horizontal plane, SPD incident at a vertical plane for a viewer, NIF parameters under unobstructed sky, and NIF parameters at the viewer's eye.

3.3. Example of practical application

We tested the workflow with a practical application, and evaluated the temporal changes in estimated NIF stimulation from daylight under two scenarios: 1) an unobstructed sky; 2) an observer's indoor view.

A generic shoebox room furnished with six workstations was used in this test case. The physical and optical characteristics of the room were defined for a previous study [60]. The room was equipped with two South-oriented windows and was simulated for the coordinates of London, during the solstice and equinox days (21 Dec, 21 Mar, 21 Jun, 23 Sep), from 07:00 to 19:00 hours for an observer seated facing the window (Fig. 5).

Due to the current gaps in standardized procedures for simulating spectral BSDFs (bidirectional scattering distribution functions), the windows were not equipped with shading systems and the contribution of the glazing to the spectral distribution of light was not included in the estimation of NIF metrics. We used the Perez sky model [36] for the evaluations, although a user can alternatively choose to run the simulations under a CIE standard sky [37]. It is worth mentioning that the models fail at negative solar altitudes (pre-dawn or post-dusk hours), hence for example NIF data could only be evaluated between 09:00 and 16:00 hours on the winter solstice. Relative-combined SPDs were calculated under an unobstructed sky hemisphere and at the observer's view. Fig. 6 presents the shifts in peak SPD value in the pre-noon hours on the spring equinox. SPD is observed to shift from the blue wavelength

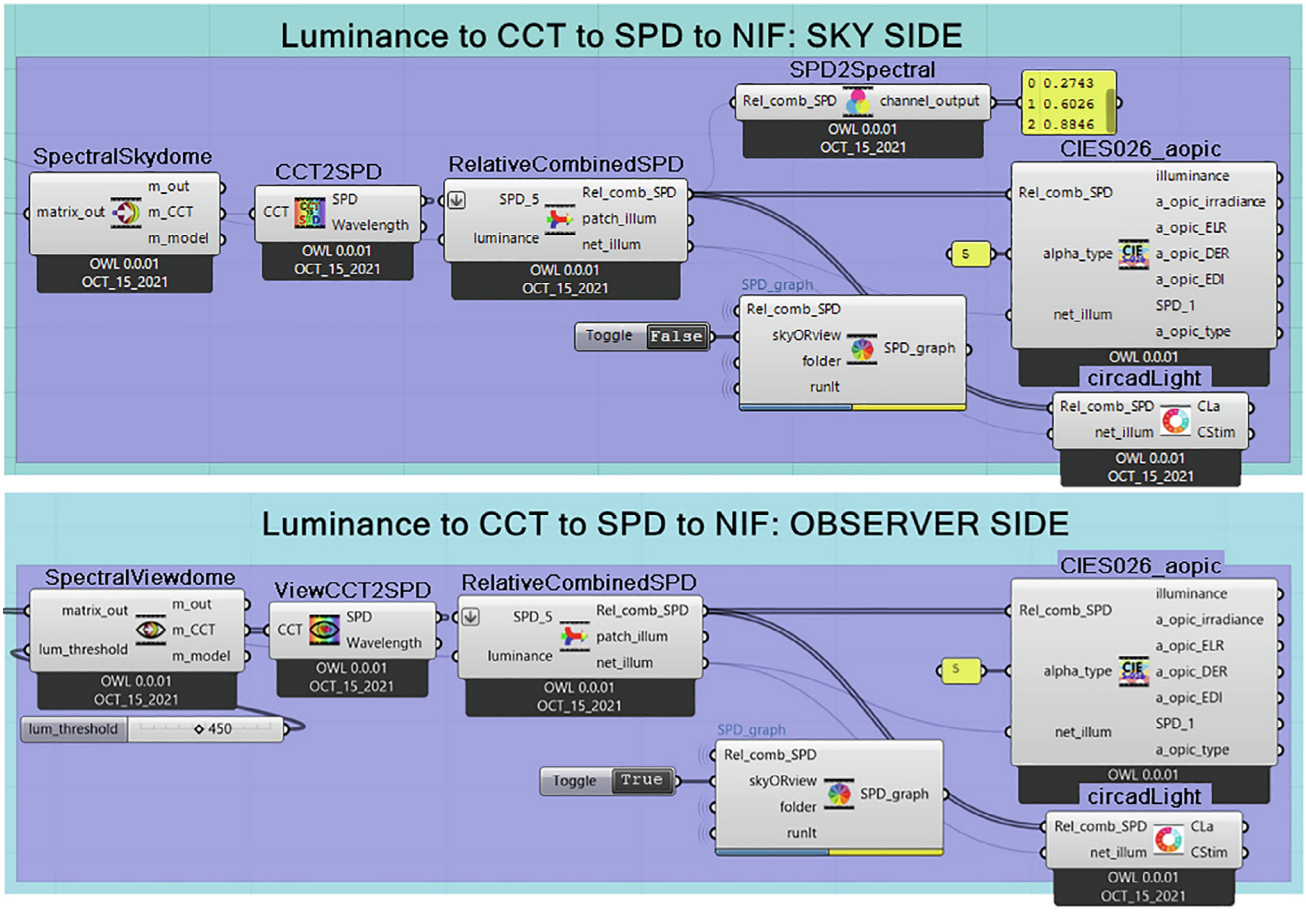


Fig. 3. Components of the Luminance-to-NIF workflow for the sky (top) and view components (bottom).

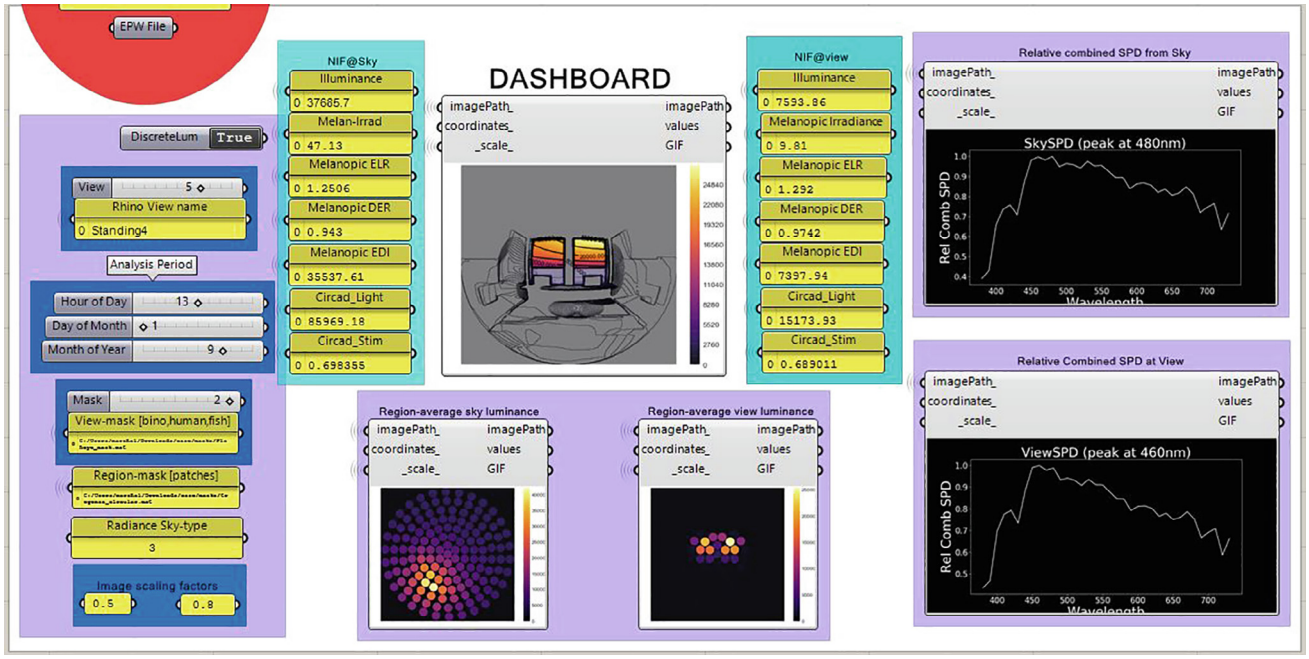


Fig. 4. Dashboard with inputs and outputs.

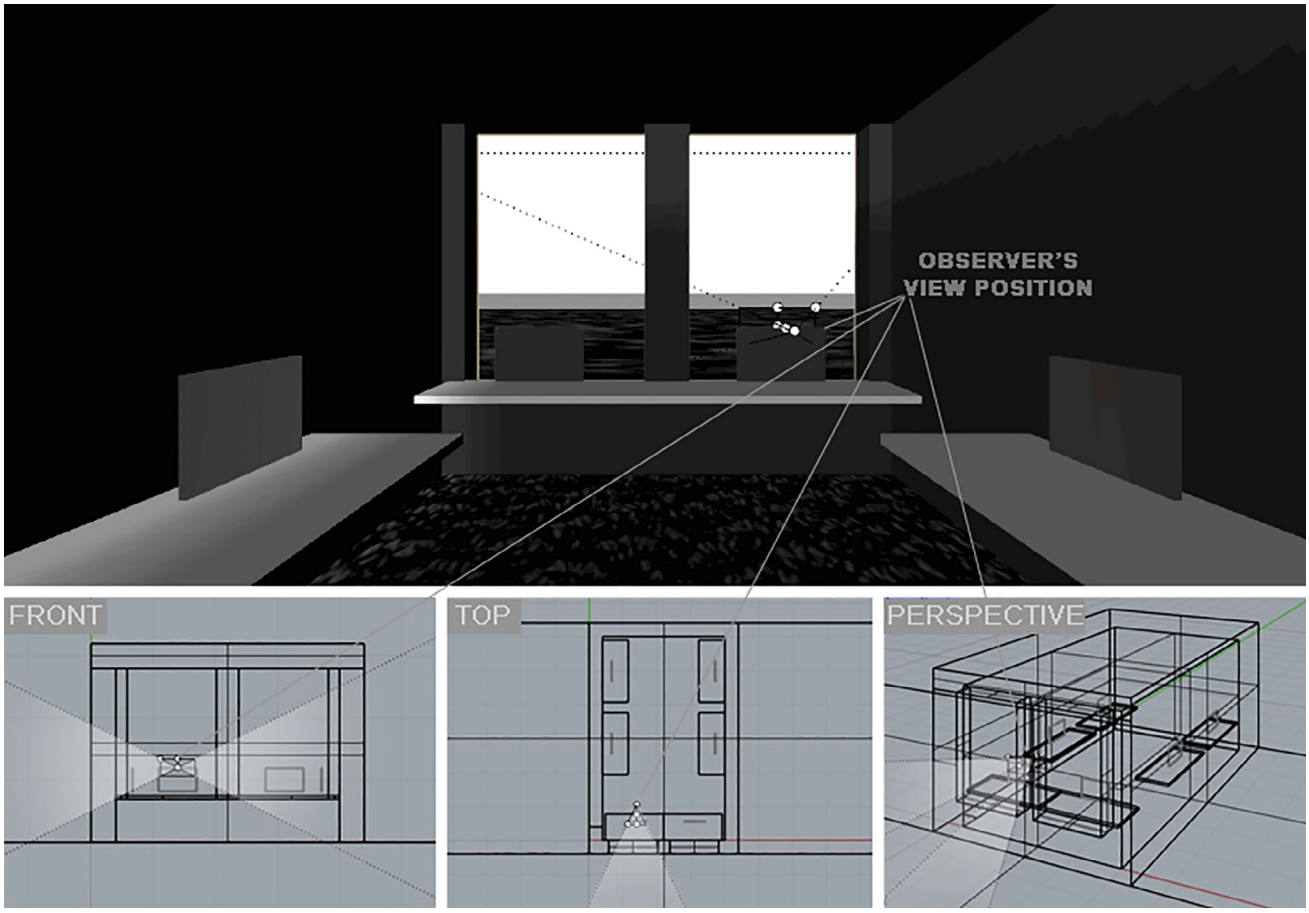


Fig. 5. Viewing position of the observer in the test room, shown from various angles.

region (peaking at 410 nm at 07:00) in the morning, to red wavelengths near noon (peaking at 460 and 670 nm, respectively for outdoors and indoors, at 13:00).

The M/P ratio (referred to as 'new M/P ratio' by Schlangen and Price [13]) was calculated from the α-opic DER (melanopic *Daylight*

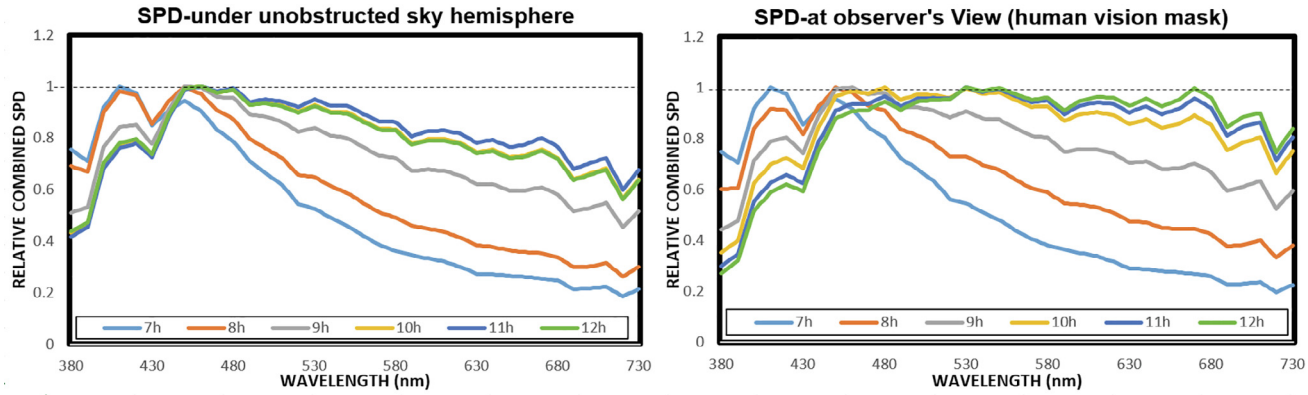


Fig. 6. Shifts in SPD peaks on 23rd September: under an unobstructed sky (left) and at the observer's view (right).

Efficacy Ratio, denoted as $E_{v,mel}^{D65}$) outputs of *CIES026_aopic*, whereas the *Circadian Stimulus* (CS) was derived from the *CStim* output of *circadLight*. The Melanopic DER is normalized to 1 for the reference illuminance D_{65}. Fig. 7 presents hourly outcomes for the selected days under an unobstructed sky and for the occupant's view position (with human-vision mask).

A high M/P ratio (greater than 1) is associated with blue-dominated SPD, and this is observed under an unobstructed sky at earlier (07:00 to 09:00) and later parts (after 15:00) of all selected days (Fig. 7a). A higher M/P ratio is also observed under the sky dome on the winter solstice, as compared to other selected days, due to prevailing overcast conditions and reduced occurrence of direct sunlight. The south facing view receives direct sunlight at an angle close to the foveal position from 09:00 to 16:00 hours on selected days. High luminance is associated with low CCT, which leads to a red-shifted SPD and, thus, a low M/P ratio (less than 1) is detected at the view position throughout the analysis period, except for the winter solstice (Fig. 7b).

Comparing the M/P ratio between the view position (vertical) and under an unobstructed sky (horizontal), the proximity of the sun closer to the foveal position for a south facing view results in a lower M/P ratio detected for the internal view, even if the value of mEDI is lower indoors as compared to outdoors. The M/P ratio, however, is just a relative indicator of the SPD potential for circadian effects, while many other factors (e.g., absolute illuminance, exposure times, etc.) clearly also need to be considered. The Circadian Stimulus is limited between the minimum threshold of 0.1 to the saturation value of 0.7. A CS exposure of 0.3 or greater at the eye in the early part of the day is considered effective in simulating the circadian system, and is associated with better sleep and mood

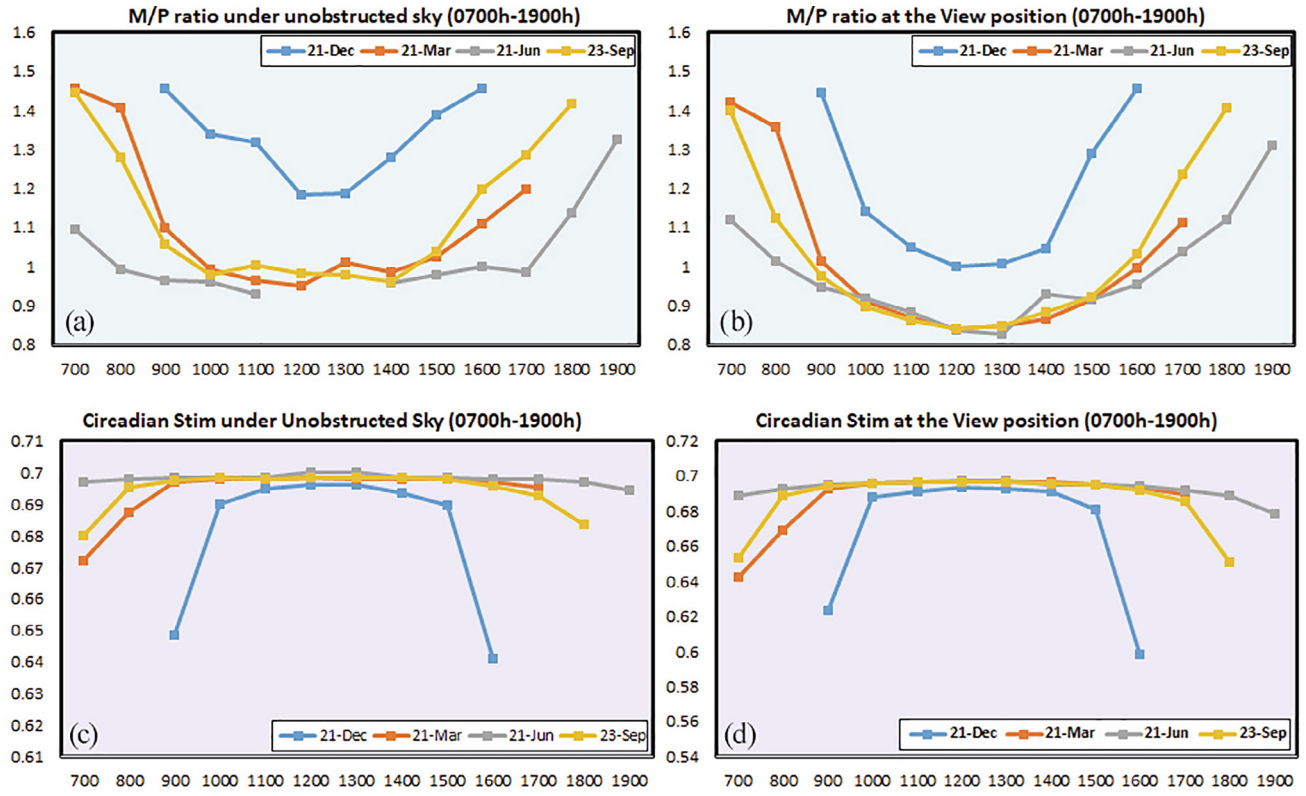


Fig. 7. Hourly variation in M/P ratio and CS for the selected days.

[15]. In our test case, proximity to the south facing window provides ample CS values (close to saturation) through the daylit hours for most of the year.

4. Discussion

Buildings account today for a great share of energy use and CO_2 emissions [61]. To increase the efficiency of our built environment, and curb environmental impacts, there is an urgent need to combine low-energy design and operation criteria with a more robust prediction of indoor environmental exposures and the consequent reactions and behaviours of building occupants. This can offer a significant contribution to reduce the performance gap that still exists between modelled and measured energy demands [62–64].

The complex processes that drive people's responses to environmental stimuli, in fact, have not yet been fully characterized [27]. This leaves important questions on how indoor spaces are effectively perceived by their users, and how such perceptions inform and drive occupants' interactions with environmental controls (e.g., blinds, electric lights, thermostats, ventilation, etc.) [65,66]. This is a matter of extreme concern, as a more robust modelling of users' responses would not only allow to predict buildings' energy performance in use more accurately, but it would also contribute to define the design and operational strategies that can lead to more comfortable and healthy user experiences. Yet, achieving (nearly) zero energy buildings and, at the same time, satisfying the demands for occupants' subjective instantaneous comfort – as well as their health and well-being over time – may require a radical step-change from current practices [67].

The design principles and operating criteria that can satisfy the demands of building users – and fully enhance their physical, physiological, and psychological well-being – might at times diverge from the typical climate-responsive strategies conducive to energy performance. In fact, research suggests that, although many parameters of indoor environmental quality (IEQ) are regulated by building standards to attain energy efficiency and meet users' demands, occupants are seldom consistently satisfied with the environmental conditions to which they are exposed [68]. There could be different reasons for this. Among these, many building standards share similar limitations, having been developed from data gathered under tightly controlled conditions, or being based on static, monotonic, and linear, dose–response relationships [69]. Similarly, many design and operation models tend to neglect the inter- and intra-individual variability in perception and subjective evaluation that drive users' needs and preferences, and the highly dynamic and variable nature of the actual conditions to which people are exposed in their built habitats [70].

In daylighting, as already mentioned, although several methods exist to predict horizontal daylight distribution based on annual climate data (CMBD, Climate-based Daylight Modelling) [71] and, to a certain extent, the probability of occurrence of phenomena such as discomfort glare [72,73], there is a significant need to improve our capacity to predict human responses to luminous stimuli from the perspective of non-visual photoreception [13]. A more robust modelling of the potential non-image forming effects of light – and a clearer characterization of how exposure to daylight inside a building, at different times of the day and year, and under different luminous intensities and spectral qualities, influence users' circadian health – can more strongly support the prediction of how they will behave in a space and how they will control shading and lighting systems to feel more alert, to decrease their sense of sleepiness, to increase their mood [74], and to perform better throughout a day [75,76]. This can have a great significance to enable a more granular modelling of indoor energy balances, and – via the implementation of more adapted and integrated building design and operation strategies – lead to more energy efficient, comfortable, and healthy buildings.

This is the motive for the development of OWL as an open-source workflow and tool, wishing to contribute towards bridging the gap between the swift theoretical advancement of knowledge in the NIF effects of light and the respective simulation capabilities. Of course, this is only the first step of a larger ambition to generate more robust and versatile design and modelling concepts, beyond conventional visual comfort issues. Based on the characteristics of climate, building typology, and occupancy, the ultimate aim is effectively to define adequate strategies to balance lighting energy use with the comprehensive needs of users, while also connecting daylighting and electric lighting systems and controls within more integrated solutions.

In fact, although the example of practical application presented in this paper has focused solely on the direct component of daylight – this often representing the dominant light source in most working environments, the OWL tool has been scripted to flexibly accommodate the contribution of multiple luminous sources, natural and artificial, and of internal and external reflections, towards a comprehensive estimation of the non-image forming effects of light. This *integrative* approach will combine the incident illuminance and specific SPD of individual light sources with the contribution from the sky to evaluate an overall relative-combined SPD, and therefore compute α-opic and circadian metrics (via the *CIE-S026_aopic* and *circadLight* components, respectively). At the same time, the spectral transmissivity and reflectivity data of various materials that are currently available in the literature will be used to perform limited-channel Radiance simulation within wavelength thresholds of melanopic curves. These developments of OWL are currently being tested and validated, and will be described in future publications.

5. Conclusion

This paper has presented the structure of a new open-source workflow and simulation tool, *OWL - Occupant Well-being through Lighting*. The tool has been originally scripted to more easily and rapidly estimate the spectral power distribution (SPD) of the sky dome from an observer's point of view inside a space at any location and time, and allow the calculation of various NIF metrics that are relevant to estimate the 'spectral diet' of building occupants [70]. The tool, alongside its workflow, responds to an existing gap in the literature, significantly extending the computational capabilities of available simulation platforms. Among other features, the tool addresses the challenge of calculating spectral data for dynamically changing sky conditions, generating relative-combined SPD from weather data by integrating existing models and protocols. Further to this, since the SPD at a view from an internal space is affected mainly by the exposed positions of the sky, the tool proposes a method for evaluating discretized luminance at the scene through image-based simulations, evaluating the SPD and the NIF potentials of a space.

Before the tool and workflow can be fully transferred to the practice of building performance simulation, however, some limitations need to be acknowledged and addressed. For example, due to the lack of guidelines for generating spectral and spatially resolved data for building materials [77], the current version of the tool is limited to using only the direct sky component of luminance, and does not consider inter-reflections. Also, the current workflow only considers the role of daylight in evaluating NIF metrics. Nevertheless, other light sources can be easily incorporated in the calculation procedure, knowing their SPD and illuminance contribution at the receiving target. With deeper understanding of spectral aspects of reflection and transmission in the scientific

community, ongoing tool developments are overcoming these shortcomings. Further to this, with greater characterisation of spectral skies through ongoing research (e.g., the recently-launched CIE Technical Committee 3–60), correlations could be developed between the indoor and outdoor SPDs (similar to the Daylight Coefficient in 2-phase or 2-phase DDS approach for Radiance simulations [78]), while further advancements of the tool could also incorporate grid-based evaluations of NIF metrics. These efforts will allow expanding OWL towards evaluating more comprehensively our energy and luminous environments and supporting more integrated daylighting and electric lighting solutions.

Declaration of Competing Interest

The authors declare to have no direct or indirect conflict of interest with the work presented in this paper.

Acknowledgements

This research was supported by a postdoctoral fellowship (n. 40000322) granted to the first author by the FNRS - Fonds de la Recherche Scientifique (Belgium) for the project SCALE (Shading Control Algorithms from Luminance-based Evaluations). Participation to IEA SHC Task 61 / EBC Annex 77 of the last author was supported by the Sector of Science and Technology (SST) of the Université catholique de Louvain. The OWL tool, the workflow documentation, and video tutorials, are all freely available for download at: https://marshalmaskarenj.github.io/OWL_Web/index.html

References

[1] P. Khademagha, M.B.C. Aries, A.L.P. Rosemann, E.J. van Loenen, Implementing non-image-forming effects of light in the built environment: A review on what we need, Build. Environ. 108 (2016) 263–272.
[2] M.S. Rea, M.G. Figueiro, J.D. Bullough, Circadian photobiology: An emerging framework for lighting practice and research, Light. Res. Technol. 34 (3) (2002) 177–187.
[3] A. Martínez-Águila, A. Martín-Gil, C. Carpena-Torres, C. Pastrana, G. Carracedo, Influence of circadian rhythm in the eye: Significance of melatonin in glaucoma, Biomolecules 11 (3) (2021) 340.
[4] C.A. Czeisler, J.F. Duffy, T.L. Shanahan, E.N. Brown, J.F. Mitchell, D.W. Rimmer, J. M. Ronda, E.J. Silva, J.S. Allan, J.S. Emens, D.-J. Dijk, R.E. Kronauer, Stability, precision, and near-24-hour period of the human circadian pacemaker, Science 284 (5423) (1999) 2177–2181.
[5] S.W. Lockley, J.J. Gooley, Circadian Photoreception: Spotlight on the Brain, Curr. Biol. 16 (18) (2006) R795–R797.
[6] M.G. Figueiro, R. Nagare, LLA Price, Non-visual effects of light: How to use light to promote circadian entrainment and elicit alertness, Light. Res. Technol. 50 (1) (2018) 38–62.
[7] R.G. Stevens, D.E. Blask, G.C. Brainard, J. Hansen, S.W. Lockley, I. Provencio, M.S. Rea, L. Reinlib, Meeting report: the role of environmental lighting and circadian disruption in cancer and other diseases, Environ. Health Perspect. 115 (9) (2007) 1357–1362.
[8] D.M. Berson, F.A. Dunn, M. Takao, Phototransduction by retinal ganglion cells that set the circadian clock, Science 295 (5557) (2002) 1070–1073.
[9] G.C. Brainard, J.P. Hanifin, J.M. Greeson, B. Byrne, G. Glickman, E. Gerner, M.D. Rollag, Action Spectrum for Melatonin Regulation in Humans: Evidence for a Novel Circadian Photoreceptor, The Journal of Neuroscience 21 (16) (2001) 6405–6412.
[10] Chang, A.M., F.A. Scheer, and C.A. Czeisler, *The human circadian system adapts to prior photic history.* J Physiol, 2011. **589**(Pt 5): p. 1095-102.
[11] J.M. Zeitzer, L. Friedman, J.A. Yesavage, Effectiveness of evening phototherapy for insomnia is reduced by bright daytime light exposure, Sleep Med. 12 (8) (2011) 805–807.
[12] R.J. Lucas, S.N. Peirson, D.M. Berson, T.M. Brown, H.M. Cooper, C.A. Czeisler, M. G. Figueiro, P.D. Gamlin, S.W. Lockley, J.B. O'Hagan, L.L.A. Price, I. Provencio, D.J. Skene, G.C. Brainard, Measuring and using light in the melanopsin age, Trends Neurosci. 37 (1) (2014) 1–9.
[13] L.J.M. Schlangen, L.L.A. Price, The Lighting Environment, Its Metrology, and Non-visual Responses. 12 (235) (2021).
[14] CIE, *CIE System for Metrology of Optical Radiation for ipRGC-Influenced Responses to Light (CIE S 026/E:2018). In. CIE Central Bureau, Vienna, Austria: Commission internationale de l'éclairage.* Vienna, Austria, 2018.
[15] M.G. Figueiro, K. Gonzales, D.R. Pedler, *Designing with Circadian Stimulus.* LD+A The magazine of the, Illuminating Engineering Society (2016) 31–33.
[16] M.S. Rea, M.G. Figueiro, A. Bierman, R. Hamner, Modelling the spectral sensitivity of the human circadian system, Light. Res. Technol. 44 (4) (2012) 386–396.
[17] LRC, *Lighting Research Center Circadian Light Combined Calculator*. 2017: New York.
[18] CIE-Div-6, *CIE S 026 α-opic Toolbox*. 2020, CIE: Vienna.
[19] Balakrishnan, P. and J.A. Jakubiec, Spectral rendering with daylight: A comparison of two spectral daylight simulation platforms, in Building Simulation 2019: 16th Conference of International Building Performance Simulation Association. 2019: Rome.
[20] Diakite-Kortlever, A., et al., *Spectral sky models for advanced daylight simulations* 2021, IEA SHC Task 61 / EBC Annex 77.
[21] Solemma, *ALFA: adaptive lighting for alertness*. 2018.
[22] M. Inanici, M. Brennan, E. Clark, in: Hyderabad, 2015, pp. 1245–1252.
[23] Roudsari, M.S., A. Smith, and G. Gill, *Ladybug: A parametric Environmental Plugin for Grasshopper to held designers environmentally conscious design*, in *Building Simulation 2013: 13th Conference of International Building Performance Simulation Association*. 2013: Chambéry.
[24] M.S. Rea, The lumen seen in a new light: Making distinctions between light, lighting and neuroscience, Light. Res. Technol. 47 (3) (2015) 259–280.
[25] L.S. Mure, F. Vinberg, A. Hanneken, S. Panda, Functional diversity of human intrinsically photosensitive retinal ganglion cells, Science 366 (6470) (2019) 1251–1255.
[26] D.M. Dacey, H.-W. Liao, B.B. Peterson, F.R. Robinson, V.C. Smith, J. Pokorny, K.-W. Yau, P.D. Gamlin, Melanopsin-expressing ganglion cells in primate retina signal colour and irradiance and project to the LGN, Nature 433 (7027) (2005) 749–754.
[27] K.W. Houser et al., Human-centric lighting: Myth, magic or metaphor?, Light Res. Technol. 53 (2021) 97–118.
[28] A.J. Zele, P. Adhikari, B. Feigl, D. Cao, Cone and melanopsin contributions to human brightness estimation, Journal of the Optical Society of America A 35 (4) (2018) B19.
[29] M. Yamakawa, S.-I. Tsujimura, K. Okajima, A quantitative analysis of the contribution of melanopsin to brightness perception, Sci. Rep. 9 (1) (2019) 7568.
[30] J.M. Zeitzer, When is a proxy not a proxy? The foibles of studying non-image forming light, J. Physiol. 596 (11) (2018) 2029–2030.
[31] IWBI, *Standard | WELL v2 Pilot.* 2021.
[32] A. Sánchez-cano, J. Aporta, Optimization of lighting projects including photopic and circadian criteria: A simplified action protocol, Applied Sciences 10 (22) (2020) 8068.
[33] K. Konis, Field evaluation of the circadian stimulus potential of daylit and non-daylit spaces in dementia care facilities, Build. Environ. 135 (2018) 112–123.
[34] Hauer, M., et al., *FACEcamp M4.4 Report on modeling procedures for non-visual comfort*. 2019.
[35] LBNL. *IGDB | Windows and Daylighting*. 2019 [cited 2021; Available from: https://windows.lbl.gov/software/igdb.
[36] R. Perez, R. Seals, J. Michalsky, All-weather model for sky luminance distribution-Preliminary configuration and validation, Sol. Energy 50 (3) (1993) 235–245.
[37] S. Darula, R. Kittler, CIE General sky standard defining luminance distributions, eSim (2002) 8.
[38] A.K. Diakite-Kortlever, M. Knoop, Forecast accuracy of existing luminance-related spectral sky models and their practical implications for the assessment of the non-image-forming effectiveness of daylight, Light. Res. Technol. 53 (7) (2021) 657–676.
[39] CIE-Div-1, *CIE 015: 2018, Colorimetry, 4th Edition.* 2018.
[40] CIE-Div-6, *CIE S026: System for metrology of optical radiation for ipRGC-influenced responses to light*. 2018: Vienna.
[41] A.K. Diakite, M. Knoop, Data-driven spectral sky models: A review, Journal of the International Colour Association (2019).
[42] Solemma, *ClimateStudio.* 2020.
[43] Piacentino, G., *GhPython | Food4Rhino.* 2017.
[44] Rahman, M.A., *GH_CPython | Food4Rhino.* 2017.
[45] Big-Ladder-Software, *EPW Data Dictionary: Auxiliary Programs.*
[46] Marsh, A., *2D Sun-path.* 2020.
[47] T. Hoffman, SunCalc - sunrise, sunset, shadow length, solar eclipse, sun position, sun phase, sun height, sun calculator, sun movement, map, sunlight phases, elevation, Photovoltaic system, Photovoltaic, 2015.
[48] Cornwall, C., A. Horiuchi, and C. Lehman, *NOAA Solar Position Calculator.*
[49] Mardaljevic, J., *Daylight Simulation: Validation, Sky Models and Daylight Coefficients*. 1999, De Montfort University.
[50] P.R. Tregenza, Subdivision of the sky hemisphere for luminance measurements, Light. Res. Technol. 19 (1) (1987) 13–14.
[51] F. Kasten, A.T. Young, Revised optical air mass tables and approximation formula, Appl. Opt. 28 (22) (1989) 4735–4738.
[52] H. Fritzsche et al., A systematic neutron reflectometry study on hydrogen absorption in thin Mg1-xAlx alloy films, Can. J. Phys. 88 (10) (2010) 723–728.
[53] Wagdy, A., et al., *Multi-region contrast method - A new framework for post-processing HDRI luminance information for visual discomfort analysis.* Proceedings of 33rd PLEA International Conference: Design to Thrive, PLEA 2017, 2017. **2**: p. 3419-3426.
[54] Inanici, M., *Per-Pixel Lighting Data Analysis*. 2005, Lawrence Berkeley National Laboratory.
[55] A. Takagi, H. Takaoka, T. Oshima, Y. Ogata, Accurate rendering technique based on colorimetric conception, Computer Graphics (ACM) 24 (4) (1990) 263–272.

[56] C. Chain, D. Dumortier, M. Fontoynont, A comprehensive model of luminance, correlated colour temperature amd spectral distribution of skylight: Comparison with experimental data, Sol. Energy 65 (5) (1999) 285–295.
[57] C. Chain, Caracterisation spectrale et directionnelle de la lumiere naturelle: application a l Eclairage des Batiments, Vaulx-en-Velin, France, 2004.
[58] Rusnak, A., *Meranie a hodnotenie spektralnych charakteristik slnecneho ziarenia. (Measurements and evaluation of spectral sun radiation characteristics, Translation by Dr. Darula)*. 2014, Slovenska Technicka Univerzita v Bratislave, Slovenia.
[59] G. Ward, R. Mistrick, E.S. Lee, A. McNeil, J. Jonsson, Simulating the daylight performance of complex fenestration systems using bidirectional scattering distribution functions within radiance, LEUKOS - Journal of Illuminating Engineering Society of North America 7 (4) (2011) 241–261.
[60] Deroisy, B., M. Maskarenj, and S. Altomonte, Modelling solar shadings with metallic slats for optimal daylighting. What parameters should we focus on?, in Building Simulation 2021: 17th Conference of International Building Performance Simulation Association. 2021: Bruges.
[61] Eurostat. *Consumption of energy. Tables and databases*. 2020; Available from: http://ec.europa.eu/eurostat/statistics-explained/index.php.
[62] Haldi, F. and D. Robinson, *The impact of occupants' behaviour on building energy demand*. Journal of Building Performance Simulation, 2011. **4**(4): p. 323-338.
[63] J. Page, D. Robinson, N. Morel, J.-L. Scartezzini, A generalised stochastic model for the simulation of occupant presence, Energy Build. 40 (2) (2008) 83–98.
[64] P. de Wilde, The gap between predicted and measured energy performance of buildings: A framework for investigation, Autom. Constr. 41 (2014) 40–49.
[65] M.V. Bavaresco et al., Methods used in social sciences that suit energy research: A literature review on qualitative methods to assess the human dimension of energy use in buildings, Energy Build. 209 (2020) 109702.
[66] M.V. Bavaresco et al., Technological innovations to assess and include the human dimension in the building-performance loop: A review, Energy Build. 202 (2019) 109365.
[67] S. Altomonte et al., Ten questions concerning well-being in the built environment, Build. Environ. 180 (2020) 106949.
[68] S. Altomonte, S. Schiavon, Occupant satisfaction in LEED and non-LEED certified buildings, Build. Environ. 68 (2013) 66–76.
[69] M.A. Ortiz, S.R. Kurvers, P.M. Bluyssen, A review of comfort, health, and energy use: Understanding daily energy use and wellbeing for the development of a new approach to study comfort, Energy Build. 152 (2017) 323–335.
[70] F.S. Webler et al., What is the 'spectral diet' of humans?, Curr Opin Behav Sci 30 (2019) 80–86
[71] J. Mardaljevic, L. Heschong, E. Lee, Daylight metrics and energy savings, Daylight metrics and energy savings. 41 (3) (2009) 261–283.
[72] J. Wienold, J. Christoffersen, Evaluation methods and development of a new glare prediction model for daylight environments with the use of CCD cameras, Energy Build. 38 (7) (2006) 743–757.
[73] M. Sarey Khanie et al., *Gaze-Driven approach for estimating luminance values in the field of view for discomfort assessments*, in *28th CIE Session*, Manchester, UK, 2015.
[74] A. Borisuit, F. Linhart, J.-L. Scartezzini, M. Münch, Effects of realistic office daylighting and electric lighting conditions on visual comfort, alertness and mood, Light. Res. Technol. 47 (2) (2015) 192–209.
[75] A.U. Viola, L.M. James, L.JM. Schlangen, D.-J. Dijk, Blue-enriched white light in the workplace improves self-reported alertness, performance and sleep quality, Scand. J. Work Environ. Health 34 (4) (2008) 297–306.
[76] K.C. Smolders, Y.A. de Kort, P.J. Cluitmans, A higher illuminance induces alertness even during office hours: findings on subjective measures, task performance and heart rate measures, Physiol. Behav. 107 (1) (2012) 7–16.
[77] Geisler-Moroder, D., et al., *BSDF generation procedures for daylighting systems* 2021, IEA SHC Task 61/ EBC Annex 77.
[78] S. Subramaniam, Daylighting simulations with radiance using matrix-based methods, LBNL, Berkeley, 2017.